Journal of Marine Systems
November 2009, Volume 78, Supplement 1, Pages S17-S36
http://dx.doi.org/10.1016/j.jmarsys.2009.01.008

Estimating the Lagrangian residual circulation in the Iroise Sea

Héloïse Muller[a, b, c, *], Bruno Blanke[b], Franck Dumas[c], Francois Lekien[d] and Vincent Mariette[a]

[a] ACTIMAR, 24 quai de la Douane, 29200 Brest, France
[b] LPO/UBO, UMR 6523 CNRS/IFREMER/IRD/UBO, 6 avenue Le Gorgeu, CS 93837, 29238 Brest Cedex 3, France
[c] IFREMER/PHYSED, BP70, 29280 Plouzané, France
[d] Université Libre de Bruxelles, CP 165/11, 50 F.D. Roosevelt avenue, B-1050 Brussels, Belgium

*: Corresponding author : Héloïse Muller, Tel.: +33 2 98 22 47 60; fax: +33 2 98 22 48 64, email address : heloise.muller@ifremer.fr

Abstract:

In this study, the Lagrangian residual circulation in the Iroise Sea is estimated by a numerical method where the trajectories of the particles released in any given velocity field are calculated by a diagnostic tool. From their knowledge, the residual Lagrangian currents are computed over a whole number of M2 tidal cycles. The Lagrangian residual circulation is mapped from sea surface currents measured by HF radars and from the surface currents computed with the Model for Applications at Regional Scales (MARS), a regional 3D ocean model forced, here, by the Weather Research and Forecasting (WRF) regional meteorological model. In order to overcome inconvenient space- and time-variations in radar coverage, the measured radar data are interpolated, extrapolated and filtered by Open-Boundary Modal Analysis (OMA). The estimated Lagrangian residual currents are compared with real drifts derived from subsurface and surface Lagrangian drifters released in the Iroise Sea in 2005 and 2007. The residual currents are analysed in the light of the physical processes (tides, atmospheric forcing and density-driven currents) known to govern long-term transport in the Iroise Sea. The similarities between drifter trajectories and the Lagrangian residual circulation inferred from either HF radar surface current measurements or modelled velocities confirm the interest of the methodological approach and make it a reasonable candidate for adaptation to the operational forecast of long-term transport.

Keywords: Iroise Sea; Lagrangian residual circulation; Regional ocean modeling; High frequency radar data

1 Introduction

1.1 Brief description of the area

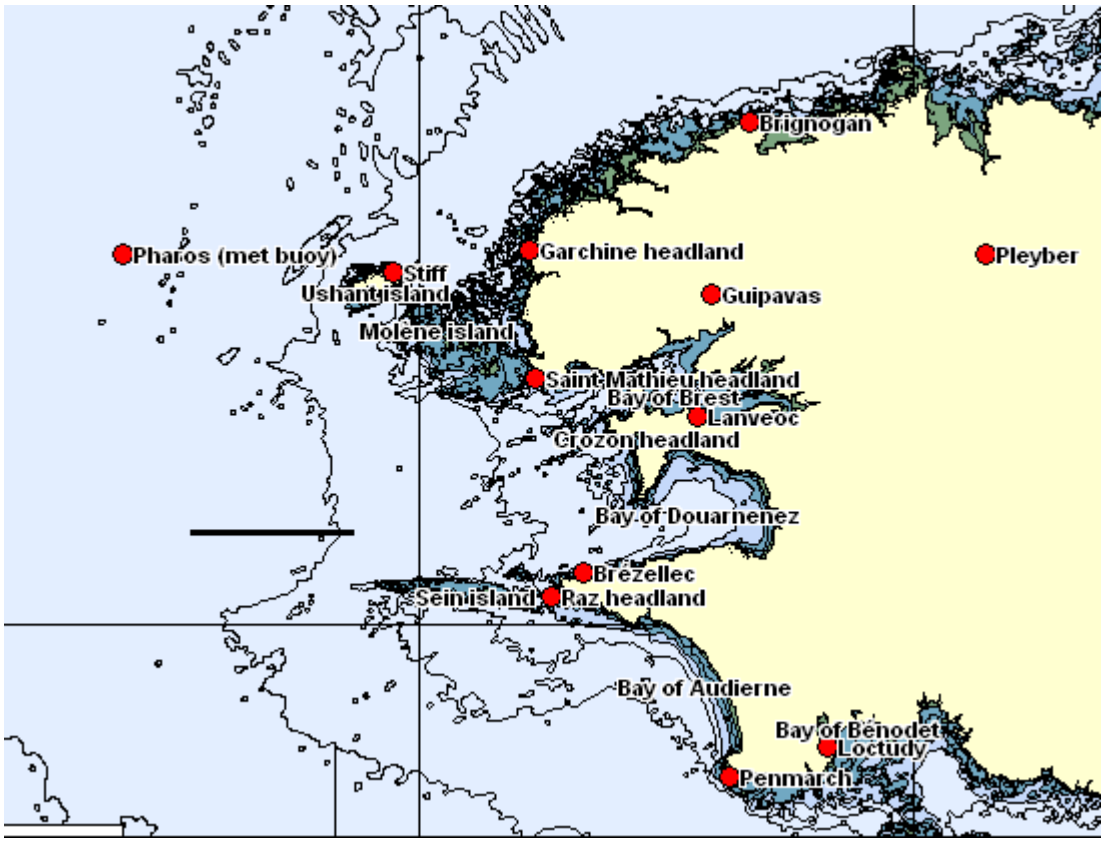

Fig. 1: Map of the Iroise Sea and Finistère with the location of the transect (in black) realised during the Fromvar campaign in September 2007 (see part 1.3.3)

The Iroise Sea is the name given to the part of the Atlantic Ocean to the west of the western end of Brittany (France) (see Figure 1). This shallow area (110 m as mean depth) is very complex in terms of dynamics and hydrodynamics because of its topographical irregularities, the presence of strong tidal currents as well as its particular geographical location along the route of low-pressure atmospheric systems. Indeed, it is subject to semi-diurnal tides and exhibits strong tidal currents (up to 8 knots in spring tide) as well as wind-generated currents. In summer, tidal fronts are generated in transition zones located between the coastal area, where the whole water column is efficiently mixed, and the offshore ocean, which is stratified because tidal currents are weaker and tidal mixing is unable to reach the surface. The strong thermal gradients in these frontal regions produce a density-driven circulation that can preponderate over the barotropic tidal current. All of these physical processes govern the short- and long-term circulations in the Iroise Sea.

The Iroise Sea is always under threat of pollution because of the very important maritime traffic. Moreover, its frontal regions are the site of intense biological activities. For these reasons, a better understanding of the long-term transport of water particles is of paramount importance in this region. It is the crux of successful prediction about the trapping of nutrients, chemicals, pollutants and microorganisms.

1.2 Lagrangian frameworks

1.2.1 Theoretical approaches

The concept of mass transport velocity was introduced by Longuet-Higgins (1969), who showed the limitations of an Eulerian point of view to explain the long-term transport of water particles: he defined the mass transport velocity as the sum of the Eulerian residual current and the Stokes drift by carrying out a first-order approximation of the Lagrangian residual velocity. Zimmerman (1979) as well as Cheng and Casulli (1982) showed the inadequacies of the Stokes formulae to explain the Lagrangian nature of residual currents. They defined the Lagrangian residual current as the displacement of a water particle divided by the corresponding time interval, which means that the Lagrangian residual current depends on the time at which a particle starts to move. To express more concretely this idea, Feng (1986) studied, at a greater order, the solution of the residual Lagrangian current and demonstrated the existence of a third term linked to the tidal phase and called by him the Lagrangian drift. These mathematical developments were all based on the linearization of the dynamics of the M2 tidal component, but they are not valid for strongly non-linear systems because they neglect higher harmonics and wind effects. Delhez (1996) generalized the first-order expression of the Lagrangian residual transport velocity while underlining that the only hypothesis necessary for such a development is to have periodic velocities with a zero mean.

1.2.2 Numerical approaches

For strongly non-linear systems, numerical methods based on particle tracking enable calculation of the Lagrangian residual circulation. For example, the one developed by Orbi and Salomon (1988) to perform Lagrangian calculations in a system of barycentric coordinates relies on the computation of particles trajectory over one tidal cycle from the velocity field of a 2D ocean model where wind forcing is ignored and only the M2 tidal component is taken into account. The particles are released every hour over one tidal cycle to get a wide spatial coverage for the Lagrangian residual velocities. Actually, the particles released at a same location, but at different times, follow different trajectories individually associated with a specific Lagrangian residual vector computed from the distance between the initial and final positions. This is why these authors chose to allocate the Lagrangian residual current to the gravity centre of the trajectory despite the existence of a beam of vectors at the initial points of release. A limitation of this method is that only a monochromatic tidal spectrum can be considered. Trajectory computation requires accurate interpolation of the velocity field and appropriate advection schemes to minimize the cumulative errors on the trajectory calculations. The off-line Lagrangian tool developed by Blanke and Raynaud (1997) is also based on the calculation of trajectories in gridded velocity fields: it allows a determination of the genuine Lagrangian residual circulation from velocity fields of various origins and is built with a robust advection scheme. The definition of an appropriate integration time is a prerequisite to its application to the study of the residual circulation in a tidal sea. It is worth underlining that the method used by Orbi and Salomon (1988) was only applied to ideal case-studies, and that the integration time was simply the period of the main tidal component.

Aside from the characteristic integration time linked to the complexity of a system including many tidal components, the long-term circulation is also difficult to determine because it is constrained by the bathymetry of the region, the weather conditions and

seasonality. The evaluation of the relative contribution of the different driving mechanisms (tides, atmospheric forcing and density-driven currents) to the long-term transport is, therefore, a key issue.

1.3 Trajectories of Lagrangian drifters released in the area in 1982, 2005 and 2007 in the light of concomitant tidal, meteorological and thermal conditions.

The contributions of the different physical processes governing the residual circulation in the Iroise Sea have already been the subject of investigations and sea campaigns involving the releases of surface and/or subsurface drifters (Mariette and Le Corre, 1982, Mariette et al., 1983). The surface Lagrangian drifters released in summer 2007 at a depth of 1 m are Coastal Ocean Dynamics Experiment (CODE)-type drifters (Davis-drifters); they report positions via the Argos satellite-based data collection system and are built to evolve, under wind conditions, at 10 m, lower than 20 m/s with wind gusts up to 30 m/s and wave height of about 8 m. The subsurface drifters released in 2005 and 2007 are Surface Velocity Program (SVP) drifting buoys equipped with a transmitter to send the data to passing satellites; in addition, buoys are tethered to a holey sock drogue centred at a certain depth set at 13 m in 2005 and 15 m in 2007. Their operating ranges are 0 to 25 m/s for wind speed and 0 to 10 m for wave height. These drifters (2007, 2005) are equipped with GPS receivers for positioning. Those released in 1982 were drogued at depths within 5 and 10 m with a chain of thermistors.

1.3.1 Barotropic tidal residual structures

Salomon et al. (1988) applied a barycentric method to the Iroise Sea to compute Lagrangian residual currents from instantaneous modelled barotropic tidal currents. It is worth noting that, in this experiment, only the M2 tidal component was taken into account and that the streamlines for this stationary current field were computed afterwards (see Figure 2). These investigations highlighted a northward pathway behind the islands and along the north coast as well as several eddy structures nearby the islands and headlands. During the summers of 2005 and 2007, the real subsurface drifters with holey sock drogue at a 15-m depth followed the pathways predicted by Salomon et al. (1988).

Figure 3 presents two 1-month trajectories of drifters drogued at a 15-m depth and configured to allow an update of positions every half hour. Filtered trajectories are superimposed. The low-pass filter is designed to span 3 days and eliminate nearly all of the tidal components except the eight diurnal components whose amplitude is weak (Demerliac, 1973). Similarities between these trajectories and the residual structures described by Salomon et al. (1988) are worth being noted: they consist of the northward pathway off Crozon headland, the loop around Ushant island and the pathway off the North Finisterian coast. The second trajectory highlights the presence of an attractive line off Crozon headland and located between the anticyclonic eddies off Raz headland and the cyclonic eddies nearby Molene island also described by Salomon et al. (1988). This consistency is a sign of the permanent existence of a few tidal structures, whatever the meteorological conditions or the season and density-driven currents. This remark is valid for the pathway behind the islands and along the Finisterian coast and also for some very local eddies induced by the presence of capes and islands (Salomon and Breton, 1993).

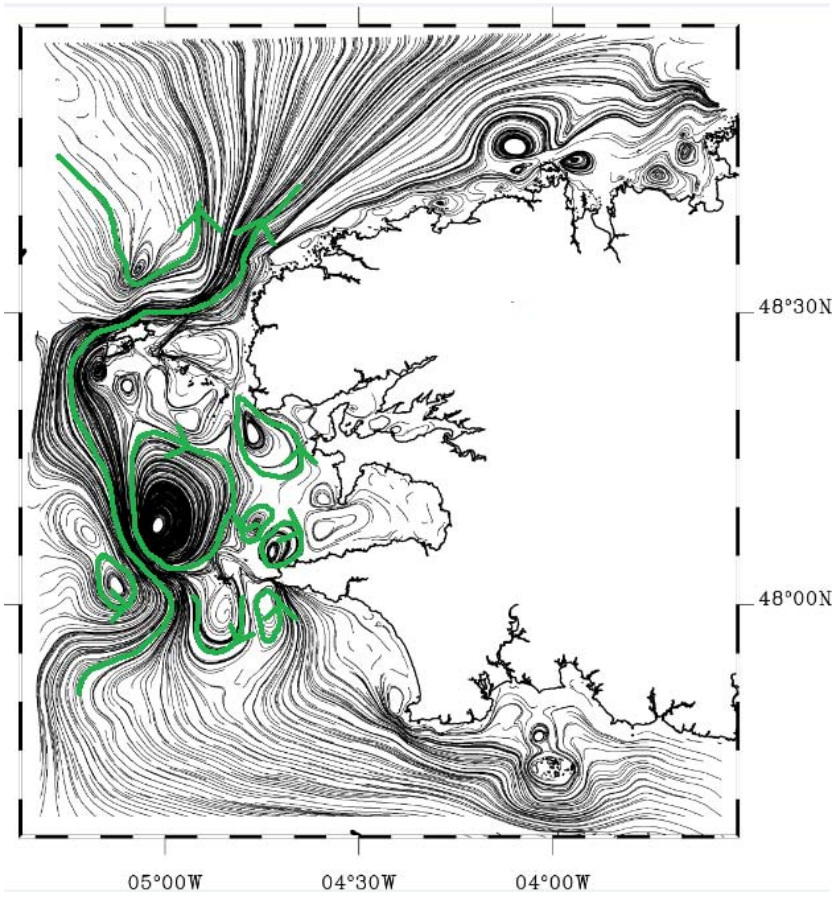

Fig. 2: Streamlines obtained from tidal residual currents following Salomon et al. (1988)

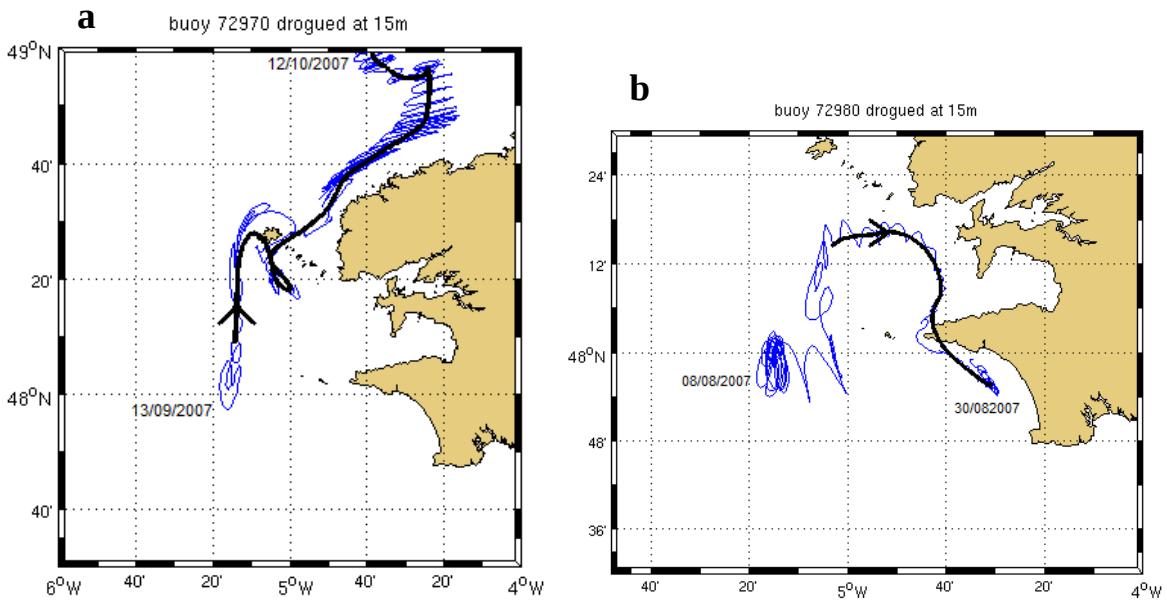

Fig. 3: Full (blue) and filtered (black) trajectories of drifters (a) 72970 and (b) 72980, both drogued at a 15-m depth

1.3.2 The residual circulation induced by wind

The superimposition of 10-m-wind vectors issued from the downscaling of GFS (Global Forecast System) analysis with the WRF model (Weather Research and Forecasting model, see part 2) reveals the impact of wind on the surface drifts. Figure 4 presents one filtered 3-week trajectory and shows that the motions are consistent with the wind direction. The portions of trajectory delimited in red are those where the agreement is poorer: two of them are in frontal regions where density-driven currents can impact Lagrangian drift, and the third one is located in channels of the Molène archipelago where tidal currents are known to prevail.

According to Jenkins (1987), the overall effect of wind and waves on the first meter of the ocean is a drift of about 3% of the wind speed at 23-30° on the right of the wind (in the northern hemisphere). This angle value is obtained for an ideal horizontally homogeneous ocean and a linear vertical turbulent mixing coefficient. Unfortunately we were unable to verify it since the situation under study, here, is much more complex. On the other hand, the mean ratio between observed and wind-derived drifts is 2% and in agreement with Ardhuin et al. (2004).

The time series of the wind and drift velocity components appear well correlated on Figure 5. The major wind events are generally correlated with the evolution of the drifter velocity, except for some gusts indicated in red in Figure 4. In the Iroise Sea, these mismatches are induced by the important role played by other driving mechanisms in some sub-regions such as frontal areas or nearby islands.

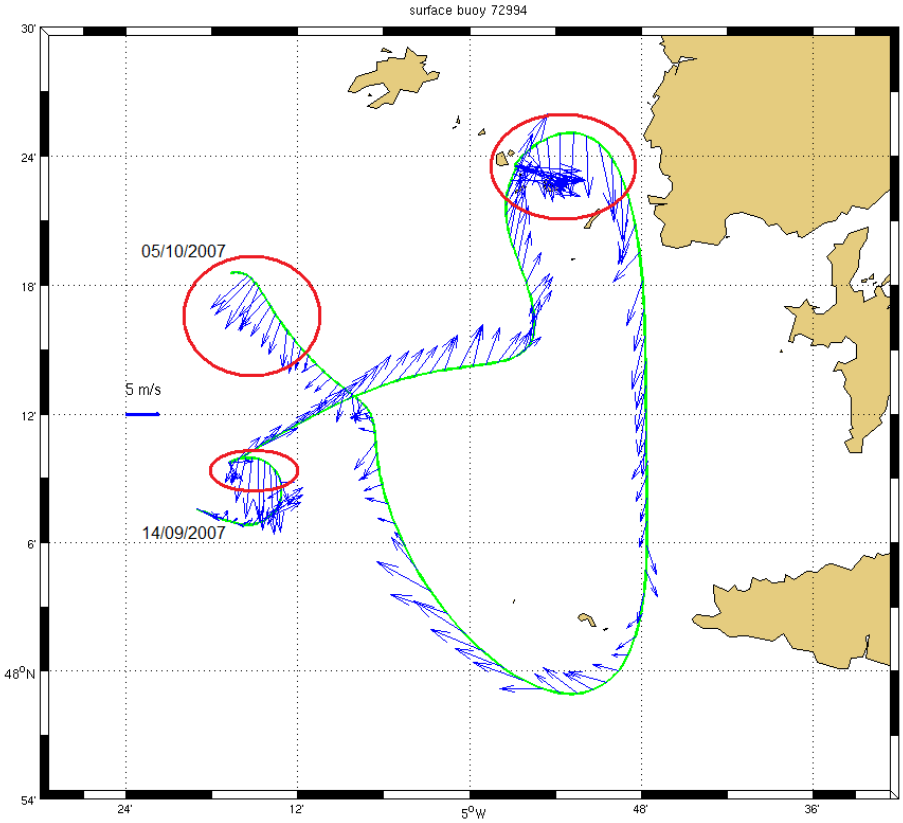

Fig. 4: Filtered trajectories (green) of surface drifter 72994 and WRF wind vectors (blue)

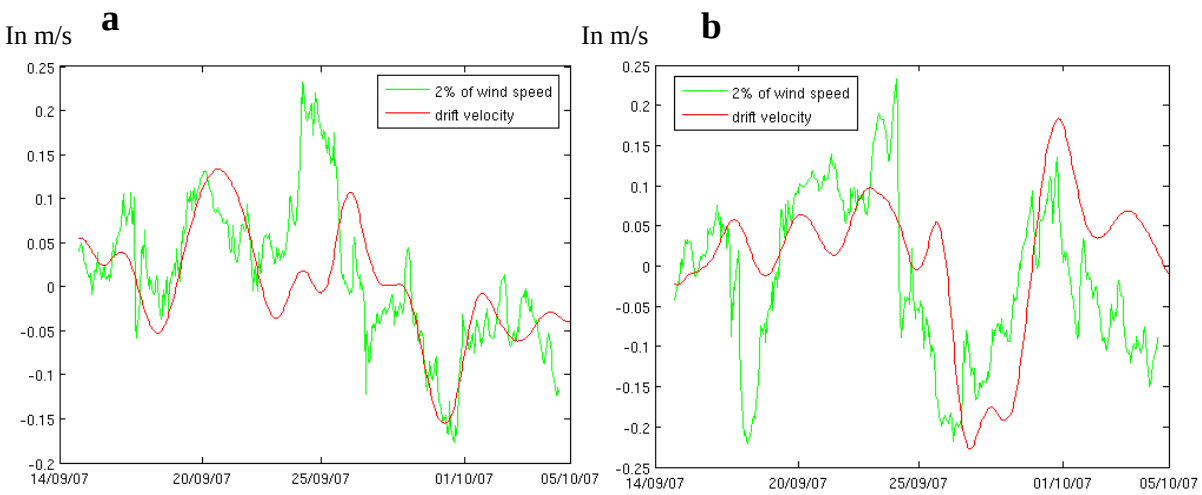

Fig. 5: Time evolution of the drift velocity of surface drifter 72994 (red) and 2% of the wind speed (green) for (a) u- and (b) v-components

1.3.3 Density-driven circulation

The trajectories followed by the surface drifters agree reasonably well with wind variability. Nevertheless, they are also sensitive to the barotropic tidal residual circulation and the density-driven circulation. Indeed, in summer, the currents generated by strong thermal gradients in frontal regions can modify the residual circulation generated by tides and wind. In the Iroise Sea, the external tidal front is thermal (Mariette and Le Corre, 1982) and was observed in September 2007 during the Fromvar experiment. The thermal wind equations and the assumption of a weak current at the sea bottom can explain the vertical profile as well as the direction of the density-driven currents.

Table 1 gives estimates of along-front and cross-front drift velocities for different drifters released in the Iroise Sea in 1982, 2005 and 2007. The drifts were computed from the positions of the drifters nearby the frontal region over 48 hours corresponding to weak wind conditions. The signs of the zonal and meridional components of the drifts are in agreement with the thermal wind rule, according to the location on either side of the front, i.e. in a homogeneous or stratified area. Under usual conditions of westward thermal gradients, the along-front drift velocity in the homogeneous region is directed northward, whereas it is southward in the stratified area, west of the front (Figure 6). The existence of the along-front circulation is noticeable on drifter trajectories at 15 m depth (Figure 7). The northward pathway along the front shown is comparable to the behaviour of the drifters studied by Mariette and Le Corre (1982), but the direction can be either northward or southward because of vertical and horizontal variations in thermocline and front positions or because of the prevailing influence of a wind gust.

Drifter number	Time coverage	Drogue depth (m)	Estimation of the currents in frontal area over 2 days				
			Period of Study	Location	Cross-front drift velocity (cm/s)	Along-front drift velocity (cm/s)	Wind direction
N2	11/09/1982-13/09/1982	between 5 and 10	11/09/1982-13/09/1982	stratified area	2.9	4.6	South-West
P2	11/09/1982-13/09/1982	between 5 and 10	11/09/1982-13/09/1982	homogeneous area	4.3	8.9	South-West
24568	6/09/2005-27/09/2005	13	6/09/2005-8/09/2005	homogeneous area	0.4	16.39	South
24748	6/09/2005-20/10/2005	13	6/09/2005-8/09/2005	stratified area	-0.6	-3.4	South
66570	13/09/2007-17/09/2007	1	13/09/2007-15/09/2007	stratified area	7.2	-15.4	North
72969	13/09/2007-6/10/2007	15	13/09/2007-15/09/2007	stratified area	4.3	-14.11	North
72970	13/09/2007-12/10/2007	15	13/09/2007-15/09/2007	homogeneous area	0.6	12.2	North
72971	13/09/2007-3/11/2007	15	13/09/2007-15/09/2007	homogeneous area	4.6	15.61	North
72982	8/08/2007-12/10/2007	15	1/09/2007-2/09/2007	homogeneous area	5.7	22.9	North-West
72992	13/09/2007-22/09/2007	1	13/09/2007-15/09/2007	homogeneous area	2.6	11.7	North
72980	8/08/2007-30/08/2007	15					
72994	14/09/2007-05/10/2007	1					

Note: the mean wind directions are issued from the model WRF for the years 2005 and 2007 and from the European Centre for Medium-Range Weather Forecasts (ECMWF) Re-analysis ERA 40 for 1982.

Table 1: Summary of the studied drifters

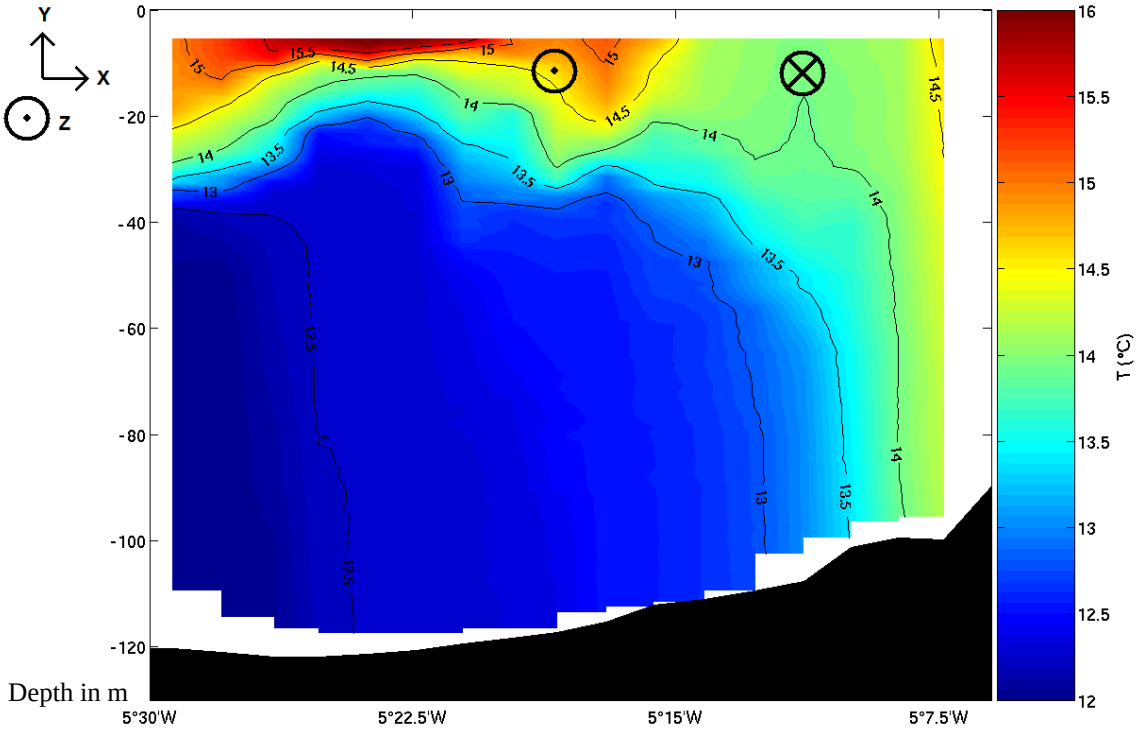

Fig. 6: Vertical temperature structure (in °C) across the Iroise Sea at 48.15°N (see Figure 1) measured during the Fromvar campaign (September 2007) and orientation of the density-driven currents from the thermal wind equations.

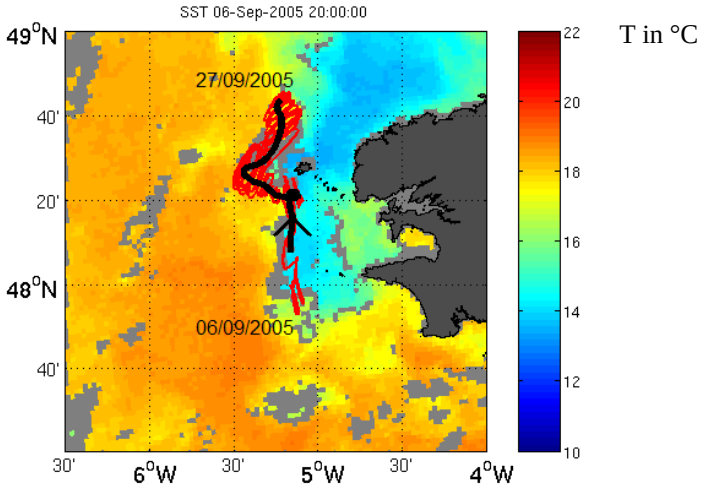

Fig. 7: SST (colour palette) and full (red) and filtered (black) trajectory of drifter 24568

2 Methodology

Lagrangian direct observations gave us some insight into the different physical processes acting on long-term transport in the Iroise Sea. However, they need to be completed by a process study based on hydrodynamical modelling to develop diagnostic tools applicable to modelled and measured velocity fields. Such diagnostic analyses will result in a more

realistic description of the Lagrangian residual circulation in the Iroise Sea further used to evaluate the respective contributions of the driving mechanisms that govern it.

Our Lagrangian analysis is applied to both ocean model outputs and genuine current measurements. Both sources of data are complementary to study the physical processes in the organisation of the Lagrangian residual circulation. The analysed sea surface currents are measured by HF radars or computed with MARS, a 3D regional ocean model in sigma coordinates, forced by high-resolution meteorological data from WRF, a regional atmospheric model. Then, the calculated Lagrangian residual currents are compared to real drifts thanks to the knowledge of the successive positions of drifters released in the Iroise Sea in 2005 and 2007 (see part 1.3).

2.1 Data and methods

2.1.1 Ground data

2.1.1.1 Surface currents measured by HF radars

The HF radar data used in this study are the projections on the zonal and meridionnal axes of the radial velocities measured by two HF WERA (Wellen Radar) radars (Gurgel et al., 2000) located at Brezellec and Garchine headlands, respectively. Each radial velocity is estimated with a precision of a few centimetres per second (Copeland et al. 1995).

Both radars emit with a central frequency set within 12190 and 12565 kHz and a bandwidth of about 100 kHz. Spatial resolution is about 1.5 km and the maximum range is 150 km. The covered angular sector is about +/- 60° with a resolution of about +/- 2° at the centre and +/- 9° at the end of the broadcast range. The radars transmit frequency-modulated continuous wave chirps with a length of 0.26 s. The values of the radial currents are computed from the Doppler spectra of the sea surface echo obtained from the integration of the scattered radio waves over several minutes (Cochin, 2006). The resulting radial currents are then reported on a regular spatial grid extending from 6.78° to 4.6°5W and from 47.30° to 49.26°N with a spatial resolution of about 2 km. The HF radar dataset from year 2005 covers the period from August to November with data collected every 12 minutes, whereas the 2007 dataset covers the year up to September with data collection every 20 minutes. The variations in radar coverage induced by its dependency upon weather and sea-state conditions make difficult the analysis of such datasets. These considerations led us to interpolate, extrapolate and filter the measurements by using Open-boundary Modal Analysis (OMA) in order to overcome such spatio-temporal variations in range and coverage (Lekien et al. 2004, Kaplan et Lekien 2007). The method uses time- and data-independent eigenfunctions that can be seen as a generalization of Fourier modes for regions with a complex coastline. At each time step, the radar data are used to determine the amplitude of each generalized mode in the reconstructed field (Kaplan and Lekien, 2007). The objective of the OMA method is threefold: first, from the discrete radar data, OMA is able to reconstruct a velocity vector everywhere in space. Second, by ignoring the modes whose length scales are below a desired threshold, OMA provides a smooth, filtered velocity field for which the degree of smoothness (i.e., the number of OMA modes) is a tunable parameter (Lekien and Coulliette, 2007). Finally, the method corrects the boundary conditions in the radar data. Whether the input radar data is tangent to the coastline or not, the output velocity of OMA will be. This property of OMA reconstructed velocity field is critical in investigating particle trajectories and Lagrangian circulation. Indeed, one must make sure that the flow is not transverse to the

coastline so as to avoid trajectories hitting or penetrating the coast, thus creating high discontinuities in the integration of trajectories (Lekien et al., 2004).

Figure 8 shows the raw (in red) and OMA-reconstructed (in black) surface currents in the region of interest. The inputs for OMA are radial measurements: the magnitude of the currents along radials joining one of the two antenna and the observed ocean point. The output of OMA is a smooth field of surface currents. Concerning the raw radar surface currents, the precision of the reconstructed zonal and meridional components depends on the angle between the two radar beams. In the case of a small angle, high uncertainties are generated on the Cartesian components.

The Comparison of the raw radar currents with the OMA surface field on Figure 8 leads to the following conclusions:

1) In the region where they overlap, the coarse total vectors usually agree with the OMA reconstructed field.
2) Near the coastline, the OMA currents usually differ from the coarse reconstruction since OMA automatically corrects the flow boundary condition.
3) On the North, South and East edges of the radar footprint, the coarse radar currents and the OMA vectors can differ significantly. In this area the radials coming from each radar antenna are almost parallel. The local method used to reconstruct the red vector is imprecise in this area and the error on the red vectors is large. On the other hand, the OMA reconstructed field is obtained by analysing the data globally and gives a better estimate that can differ significantly from the raw vectors (see error maps in Kaplan and Lekien, 2007).
4) Outside the radar footprint, OMA works as an extrapolator. For convenience, the OMA output covers the entire region but validity of the reconstructed field far away from the radar footprint should not be assumed. Outside radar coverage zone, the OMA method introduces artificial pieces of information that can be disregarded.

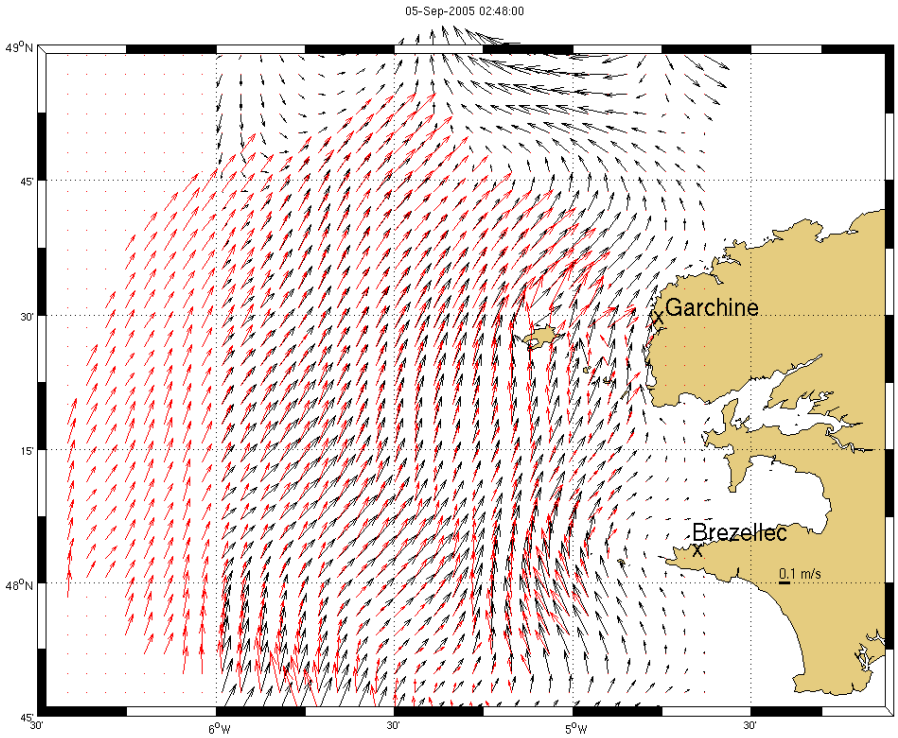

Fig.8: Surface currents estimated by raw pointwise recombination of HF radar data (red) and surface currents reconstructed with OMA (black) on September 5, 2005, 02h48; Brezellec and Garchine are the radars' locations.

2.1.1.2 Lagrangian drifters

The simultaneous availability of HF radar data and real drifter positions enabled validation of instantaneous currents as follows: the instantaneous velocity is deduced from bihourly-sampled drifter positions prior to comparison with HF surface currents linearly interpolated along the trajectories. The tidal ellipses obtained for meridional velocity components plotted as a function of zonal components show that the tidal signal captured by HF radar data and the true subsurface drifts are roughly equivalent (Figure 9). Statistics over 44 M2 tidal cycles are of the same order of magnitude for both datasets, with mean values from about 2 to 4 cm/s. The standard deviation for zonal velocity inferred from radar measurements and drifters is about 4 cm/s; it is about 21.5 and 12.3 cm/s for the meridional velocity derived from drifters and that from radar measurements, respectively. Linear correlation coefficients between HF radar surface currents and subsurface drifts are 0.67 and 0.84 for the zonal and meridional components, respectively. Equivalent coefficients calculated between HF radar surface currents and surface drifts are 0.67 and 0.83.

It is worth noting that the agreement is generally poorer for the zonal component of the drift. Indeed, in the Iroise Sea, the flow is generally directed northward and *u* is weaker than *v*, which makes its capture by HF radar more difficult. The slight discrepancy between both sources of data for the years 2005 and 2007 likely comes from i) the fact that concomitance of both datasets is only approximate, ii) the geometrical error associated with the projection of radar data in Cartesian coordinates, iii) error on the instantaneous velocities calculated from successive sampled positions along drifter trajectories. These results highlight the difficulty of comparing Lagrangian data and instantaneous measurements at fixed points. Nevertheless, the overall fair agreement makes it worth developing a method to estimate the Lagrangian residual circulation in the Iroise Sea from genuine current measurements, e.g. radar data, and results from ocean model.

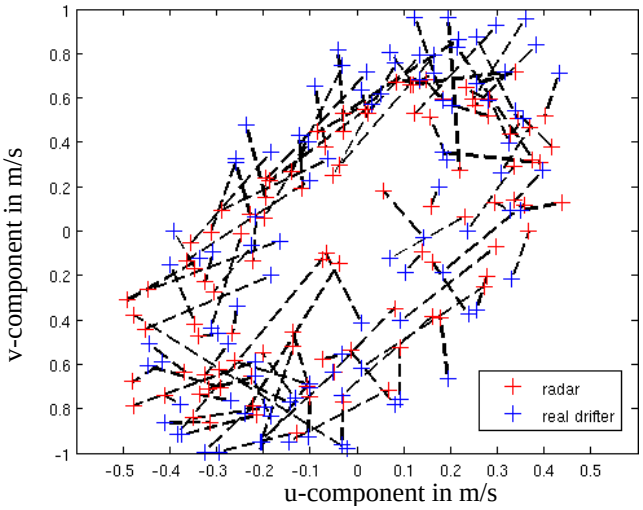

Fig. 9: Collocated HF Radar (red + symbol) and real subsurface drifter (blue + symbol) velocities showing the tidal ellipse over 5 days. Dashed segments connecting the radar and drifter velocities indicate the difference (bias) between the two velocity estimates.

2.1.2 Surface currents calculated by MARS forced by WRF

The use of a coastal, hydrodynamical numerical model is complementary to data analysis for gaining more insight into the contribution of the different driving mechanisms involved in Lagrangian residual circulation. Moreover, it is an essential tool to predict Lagrangian drifts. In this study, the modelling of the hydrodynamics in the Iroise Sea by the MARS 3D regional ocean model (Lazure and Dumas, 2007) was as realistic as possible; the numerical configuration is embedded in an intermediate 3D coarser resolution model with a mesh refinement coefficient set to 3. The parent grid provides the child one with information about temperature, salinity, velocity and free surface elevation with a 1-way nesting (Penven et al., 2004) using AGRIF tools (Adaptative Grid Refinement in Fortran, Debreu et al. 2005). The open boundary condition for sea surface height in the coarse 3D model is provided by a 2D barotropic model forced by sea surface heights from the Finite Element Solutions FES (2004) tidal atlas (Lyard et al., 2006) with 8 tidal components (M2, S2, N2, K2, P1, O1, K1, Q1). The configuration presented in this paper consists in a 5-km resolution 2D model with an intermediate 2-km 3D model embedded in it. The Iroise Sea model itself has a 667-m horizontal resolution. The present configuration (Muller et al., 2007) is original because of its off-line forcing with high resolution (2 km) data from the WRF regional meteorological model. The atmospheric fluxes are computed with bulk formulae (Luyten and Mulder, 1992) applied to WRF outputs. The meteorological data necessary for WRF initial and boundary conditions are 6-hour NCEP global tropospheric analyses available on a global 1°x 1° grid. The boundary conditions over the ocean were determined by using an atlas of SST corresponding to a 10-day climatology with a 9-km resolution calculated using night data from NOAA satellites from 1985 to 1995 (Faugère et al., 2001). It is a noticeable improvement in Iroise Sea modelling since it enhances the consistency between SST and the temperature of the atmospheric boundary layer and allows more realistic representations of heat fluxes at the air/sea interface. The Iroise Sea model is run over summer and autumn 2005 and 2007 to permit relevant comparisons with the surface currents measured by HF radars and drifters.

MARS instantaneous surface currents compare reasonably well with currents derived from HF radar data for correlation and bias, except nearby the islands where radars measurements are less reliable (Muller et al., 2007). After extraction of M2 tidal ellipses, HF coastal radar observations and MARS results also proved to be basically in phase, however with an overestimation by the model, almost everywhere, of the length of the major axis (Muller et al., 2007).

2.2 Lagrangian residual currents

The Lagrangian residual current is computed with two different methods: i) a theoretical calculation based on the Longuet-Higgins (1969) approximation and ii) the use of a diagnostic Lagrangian tool (ARIANE; Blanke and Raynaud, 1997) to compute the full trajectories of numerical particles advected in a given velocity field. The first method gives a rough estimate of the Lagrangian residual circulation deduced from the instantaneous circulation and shows the impact of the Lagrangian drift upon the transport of fluid. Thanks to the use, here, of the 2D velocity field computed by a version of MARS that takes only M2 into account and ignores wind forcing, our results are consistent with classical Longuet-Higgins studies. In the second method, the full trajectories are integrated over an appropriate period to infer the

Lagrangian residual circulation. We applied it to both model outputs and gridded current measurements inferred from HF radar data.

2.2.1 Theoretical approach

According to Longuet-Higgins (1969) and considering the 2D current field (u,v) at the point (x,y), the mass-transport velocity (u_L, v_L) is defined as:

$$v_L = \overline{v_{eulerian}}^{T} + \overline{(\int_{t_0}^{t} u d\theta) \times \frac{\partial v}{\partial x}}^{T} + \overline{(\int_{t_0}^{t} v d\theta) \times \frac{\partial v}{\partial y}}^{T} + \ldots$$

$$u_L = \overline{u_{eulerian}}^{T} + \overline{(\int_{t_0}^{t} u d\theta) \times \frac{\partial u}{\partial x}}^{T} + \overline{(\int_{t_0}^{t} v d\theta) \times \frac{\partial u}{\partial y}}^{T} + \ldots$$

where $\overline{\ldots}^{T}$ is a time average over time T, T is a multiple of the M2 tidal period and t_0 is the time when particles start moving.

This direct calculation of the Lagrangian residual current is a first-order approximation; it is valid for systems with weak non linearities. The mathematical expression shows that, for currents with fluctuations much larger than their means, the second term linked to the horizontal gradient of the velocity field (i.e. the Stokes drift) may have a key role in mass transport.

2.2.2 Numerical approach

To describe the Lagrangian residual circulation in the Iroise Sea in a more realistic way, Lagrangian diagnostics were performed with the off-line ARIANE tool suitable for water mass tracing (Blanke and Raynaud, 1997). Particles are initialized at each U- and V-point of the MARS C-grid (according to Arakawa and Lamb, 1977 classification) for u_L and v_L computations, respectively. Trajectories are integrated over a full M2 tidal cycle, the residual Lagrangian vectors are deduced from the initial and final positions of particles and allocated to the centre of mass of each trajectory. Finally, the zonal and meridional Lagrangian residual components are regridded on the U- and V-points of the MARS grid, respectively. This calculation is applied, at first, to the MARS 2D velocity field to allow comparison with the results issued from application of the Longuet-Higgins formalism. Equivalent experiments are then carried out with surface currents computed with the 3D configuration forced by the high-resolution WRF meteorological model. This stage towards a more realistic description of the Lagrangian residual circulation is relevant as far as comparisons with real data are performed. Thus, Lagrangian diagnostics are also performed with HF radar current measurements post-processed with OMA (Lekien et al., 2004, Kaplan and Lekien, 2007). Here, OMA is used to reconstruct the radar surface current field on a regular grid because original radar data have different grid characteristics and can be noisy or irregularly sampled in time.

2.3 Lagrangian view versus Eulerian view

Experiments carried out on ideal 2D periodic velocity fields are of great help to focus on the difference between the Eulerian and Lagrangian mean velocities. In this study the

relevance of a Lagrangian view was enhanced by carrying out a numerical ARIANE integration that uses 2D currents calculated by the MARS model run with the M2 tidal component alone and no wind forcing.

Figure 10 shows that the Lagrangian transport can be much larger than the Eulerian mean one, especially in frontal areas. The relative ratio of both quantities can reach 64.6 over one tidal cycle. A close examination of Figure 11 reveals differences in direction in frontal areas nearby islands and headlands as well the opposite directions sometimes shown by both velocities.

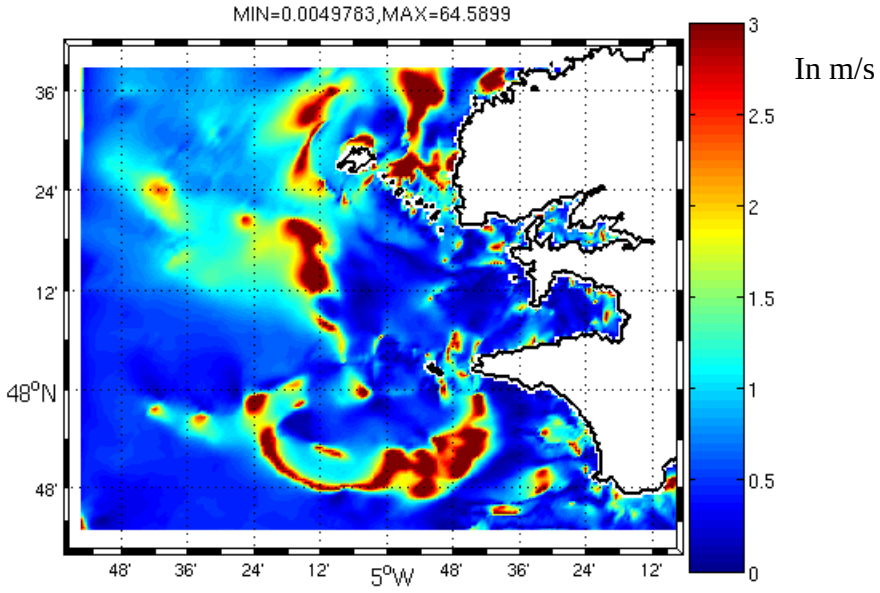

Fig. 10: Relative ratio of the mean Lagrangian and Eulerian velocity magnitudes $\frac{U_L - \overline{U_{eulerian}}^T}{\overline{U_{eulerian}}^T}$**,** $U_{eulerian}$ **is the norm of the Eulerian residual current and** U_L **is the norm of the Lagrangian residual current (note: the colour palette is saturated)**

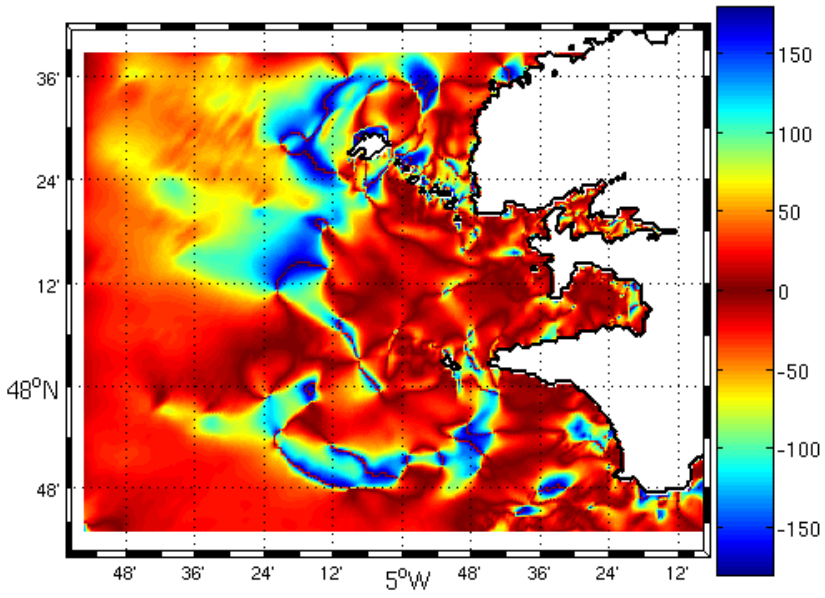

In degrees

Fig. 11: Angle in degrees between the Lagrangian and Eulerian mean velocities $\left(\theta = sign(\overrightarrow{u_{lagrangian}} \times \overrightarrow{u_{eulerian}}) \times arc\cos(\frac{\overrightarrow{u_{eulerian}}.\overrightarrow{u_{lagrangian}}}{\left\|\overrightarrow{u_{eulerian}}\right\|.\left\|\overrightarrow{u_{lagrangian}}\right\|}) \right)$

3 Results

3.1 Theoretical and numerical calculations over one M2 tidal cycle

In order to compare a numerical Lagrangian integration with ARIANE against the theoretical results from Longuet-Higgins, the two methods described above are applied to the barotropic velocity field computed with the 2D MARS model with no integration of the wind forcing, but only the M2 tidal component. In order to lie in the domain of validity of the Longuet-Higgins approximation, the following graphs (Figures 12b and 13b) hide the area with strong non linearities, where $\frac{\overline{U_{eulerian}}}{U_{\max} - U_{\min}} \leq 0.07$ and $U_{\max}$ and $U_{\min}$ are, respectively, the maximum and the minimum of instantaneous velocity, (Delhez, 1996). This area is not hidden for ARIANE results, since the numerical method gives access to the full Lagrangian displacement.

The structures captured by both methods are similar, and the orders of magnitude are nearly alike (Figures 12 and 13). The results obtained with the Longuet-Higgins approximation are more spoiled with noise than the numerical results, but they show that, away from regions of complex bathymetry and coastline, the theoretical approximation gives a fair first-order description of the Lagrangian residual circulation. Nevertheless, the Longuet Higgins approximation appears inappropriate for a thorough investigation of the long-term transport in the Iroise Sea and, thus, in the following, the Lagrangian calculations will be made with ARIANE.

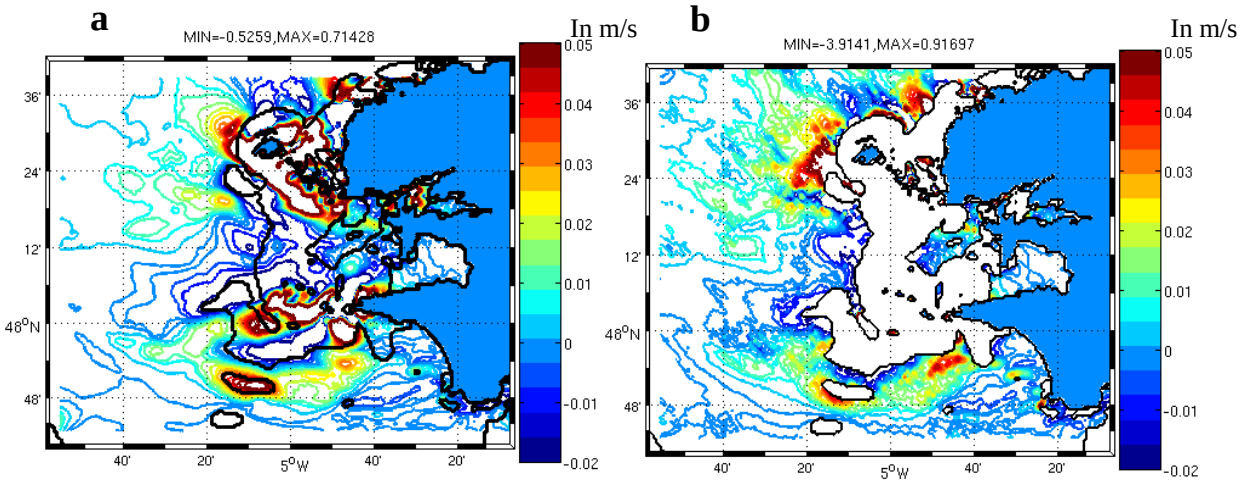

Fig. 12: Difference between the Lagrangian and Eulerian mean zonal velocities ($u_L - \overline{u_{eulerian}}^T$, in m/s) computed with (a) ARIANE and (b) Longuet-Higgins theoretical approach; area with strong non linearities is hidden in the b panel.

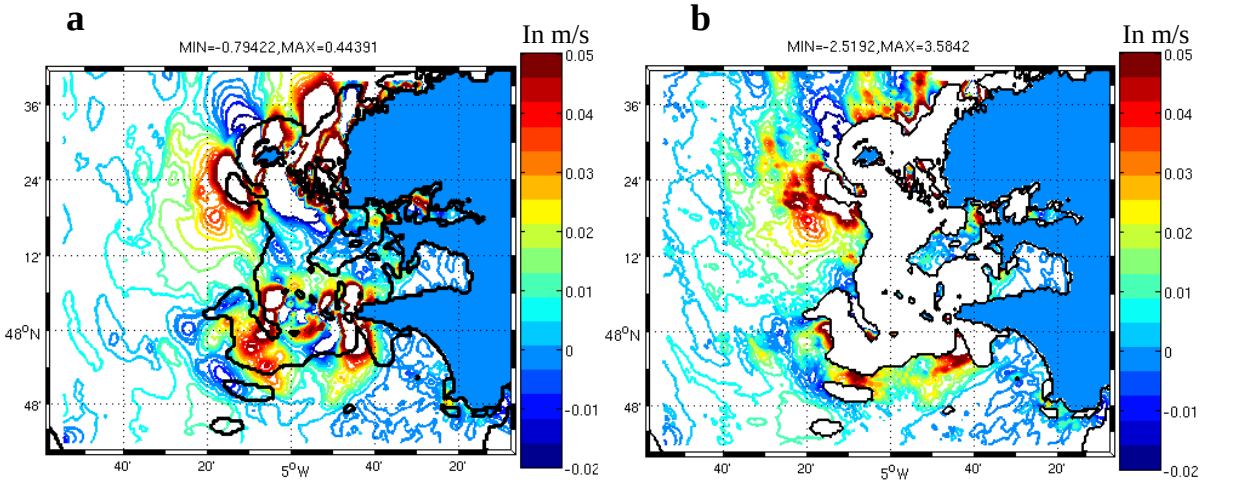

Fig. 13: Same as Figure 12 except for the mean meridional velocities

3.2 Comparisons between Lagrangian residual currents computed from model outputs and HF radar data

The method applied here to MARS 3D-modelled surface currents (same configuration as in section 2.1.2) and to surface currents measured by HF radars (Figures 14 and 15) was described in section 2.2.2. ARIANE diagnostics are derived not only for raw radar data but also for OMA post-processed data in order to test the advantage of improved and constant space and time coverage. The smoothing introduced by the OMA processing leads to significant differences in the restitution of the Lagrangian residual currents. It is worth noting that the order of magnitude of the Lagrangian velocities evaluated from raw radar data is more comparable to the MARS-based results than the velocities calculated after the OMA post-

processing. Besides, even if the structures are not at the same place, similarities between observed and modelled patterns are noticeable, especially near the islands.

The model-data comparison was worth being done using a Lagrangian framework. Indeed, an ocean model can reproduce instantaneous currents with a fair reliability, but small errors in their estimate can generate huge errors in Lagrangian transport. Moreover, whatever the accuracy of an ocean model and the atmospheric fields used to force it, it generates a significant amount of internal mesoscale and sub-mesoscale variability quite different from the one issued from direct observations. Lagrangian diagnostics run over one tidal cycle, for a period with a large radar coverage, allowed us to estimate the relevance of the OMA interpolation of radar data for Lagrangian residual current computations. Indeed, even though the residual circulation looks underestimated in post-processed radar measurements, this approach has the advantage to enable calculations over the whole period of radar measurement without needing to take into account possible failures in the time- and space-coverage by HF radars.

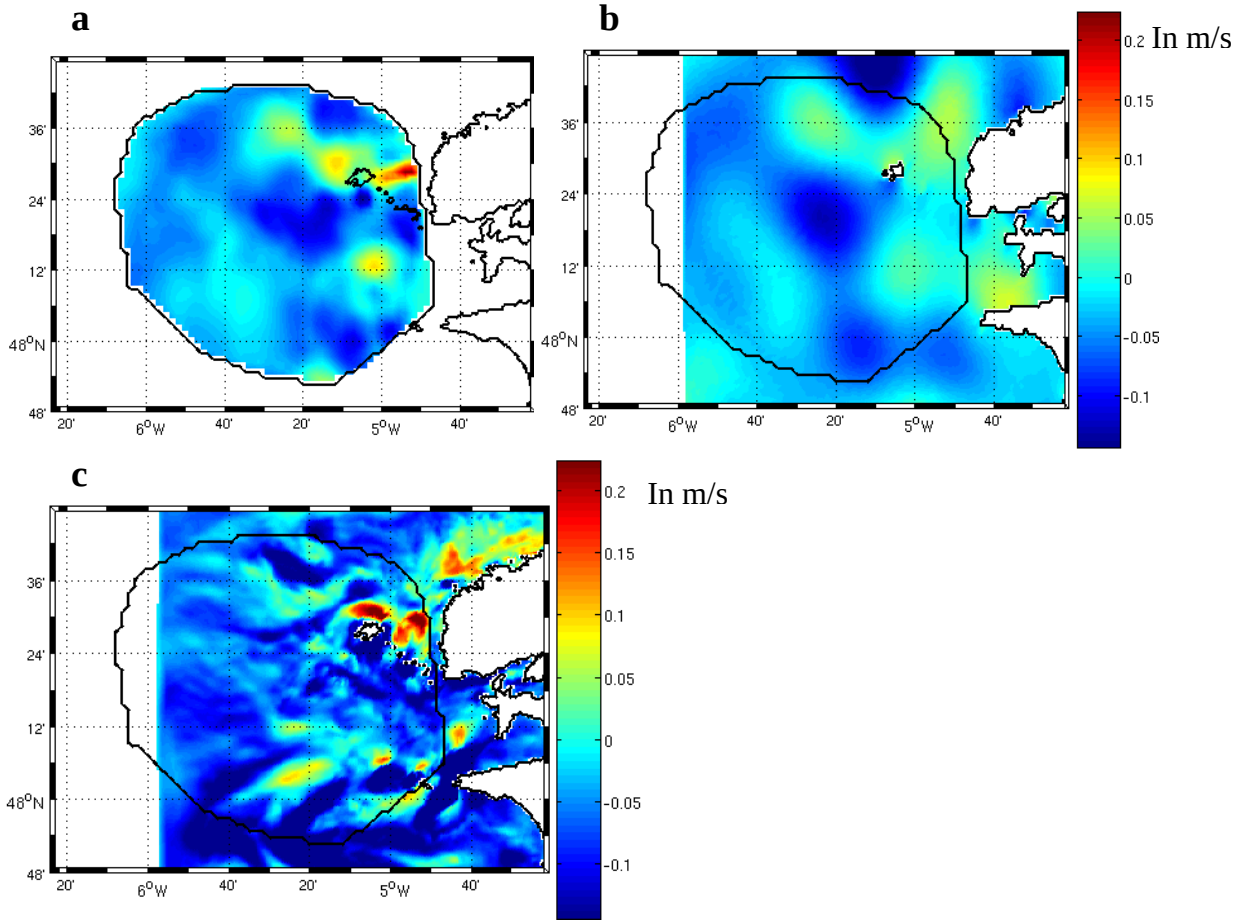

Fig. 14: Zonal component of the Lagrangian residual current calculated from (a) raw radar data, (b) OMA-post-processed radar data, (c) MARS results, computed over a M2 tidal cycle from September 12, 2005, 21:11:00 UTC; the black contour represents the HF radar coverage.

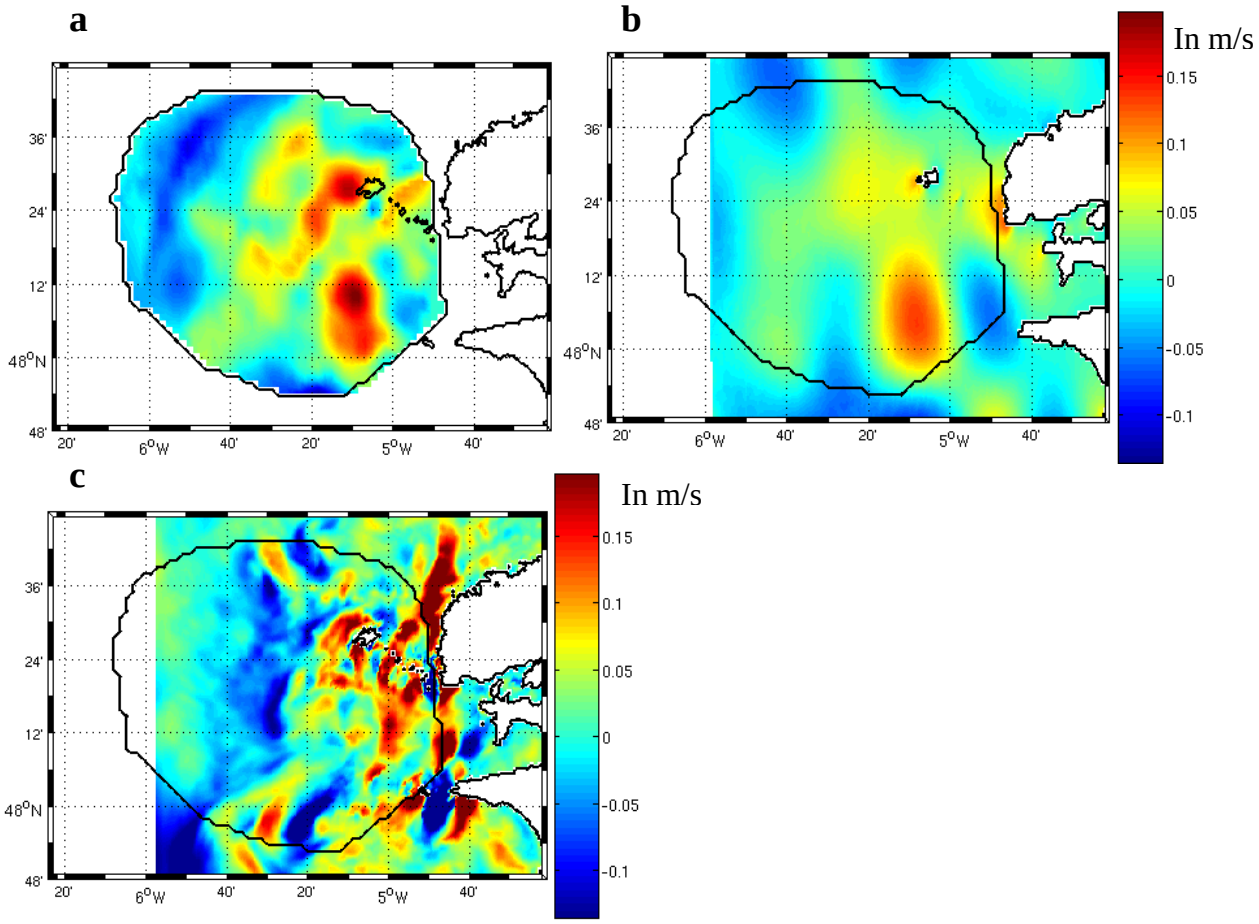

Fig. 15: Same as Figure 14 except for the meridional component of the residual current.

3.3 Process-study-oriented Lagrangian results

After this first validation of characteristics of the Lagrangian residual circulation in the Iroise Sea, it is worth analysing the results with respect to the physical processes known to govern transport in this area, i.e. mainly tides, atmospheric forcing and density-driven currents. For this purpose the results presented in this section rely on: i) Lagrangian residual circulation maps built at some key dates over one or four tidal cycles and ii) the analysis of a few relevant trajectories integrated with ARIANE.

3.3.1 Tidal residual currents

The strongest tide-related residual structures are especially obvious in the results obtained from modelled current fields. Indeed, the areas where the barotropic tidal currents are predominant are close to the coastline and out of the radar coverage (indicated by a thick black line in the following figures). Figure 16 illustrates the situation on September 18, 2005 characterised by spring tide and weak wind conditions. The model results highlight the presence of a cyclonic eddy (in the northern part of the area under study, at 5°10'W and 48°35'N) as well as a well-organised pathway along the northern coast of Finistère. It is worth

noting that this cyclonic circulation was already noticed by Salomon (see Figure 2, at 5°05'W and 48°35'N). Moreover, the eddies described by Salomon et al. (1988) between Sein Island and the Raz headland are also noticeable in Figure 18. Equivalent results obtained from radar data (Figure 17) also show the northward residual current around Molene and Ushant islands as well as cyclonic eddies to the North West of the Ushant island. Lagrangian tidal residual structures appear as rather easy to reproduce in areas where the tidal current is very strong. It is however more difficult to reproduce smaller tide-related structures between the islands and nearby headlands because of the high resolution needed for their modelling.

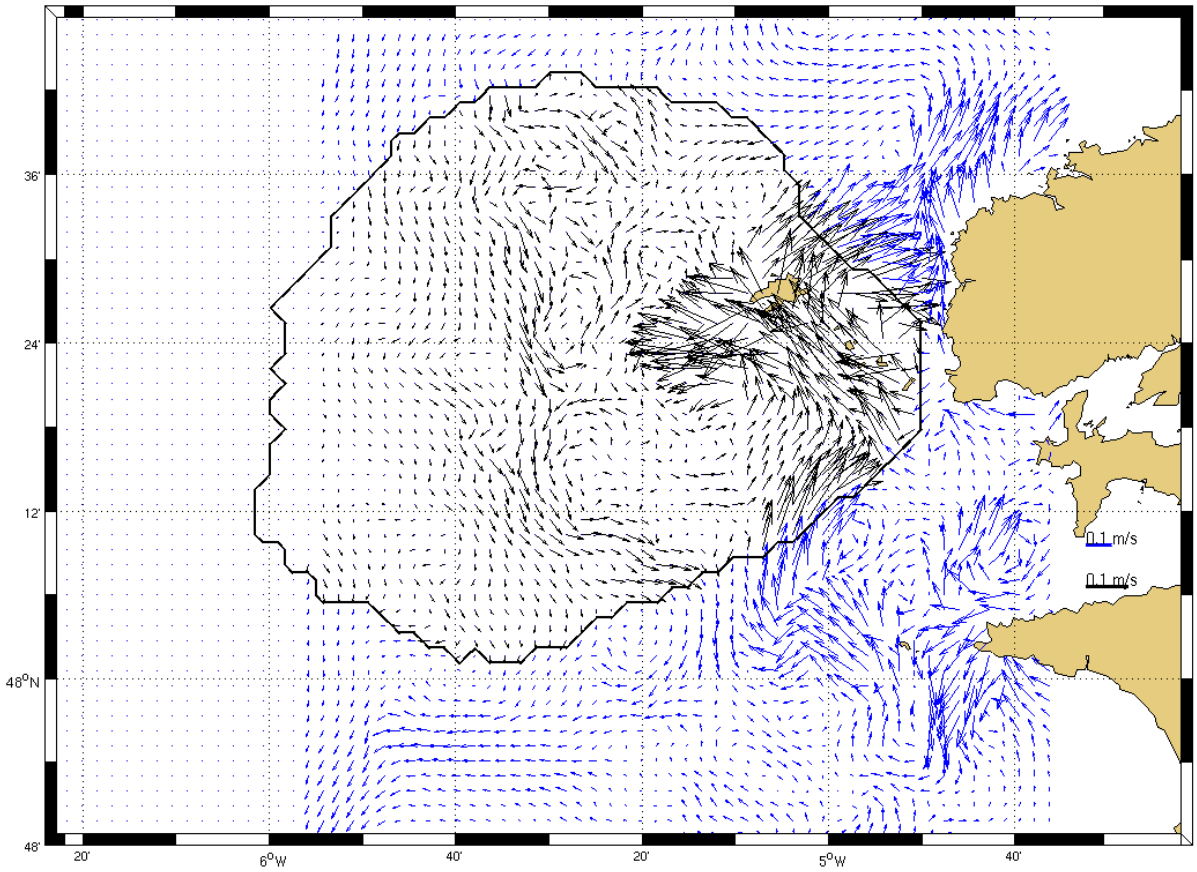

Fig. 16: MARS Lagrangian residual current over one tidal cycle from September 18, 2005, 00:00 UTC.

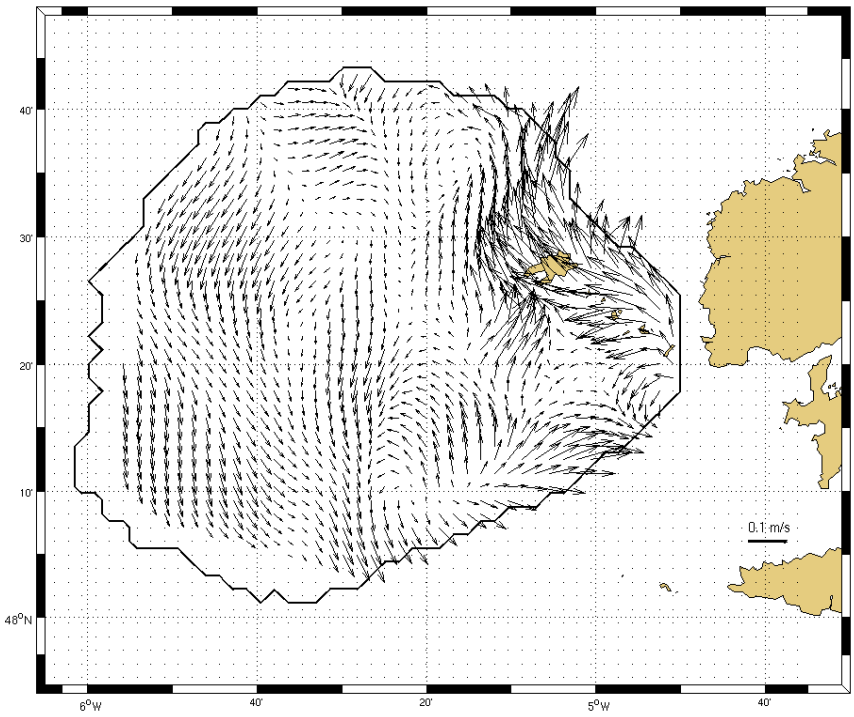

Fig. 17: HF-radar-derived Lagrangian residual current over one tidal cycle from September 18, 2005, 00:00 UTC.

3.3.2 Wind-driven drift

In order to evaluate the wind contribution to the Lagrangian residual circulation, let us focus on four consecutive tidal cycles starting on July 24, 2007, 00:00 UTC for neap tide and strong wind conditions (with a southwest WRF wind speed of 8.5 m/s on average). The Lagrangian residual circulation calculated over the same period with the modelled velocity field is in good agreement with the mean wind direction, offshore, in the stratified area (Figure 18a). The same diagnostic applied to the radar-derived surface velocity over the same period also shows an eastward uniform offshore current that deviates generally to the right of the mean wind (Figure 18b). Our WRF wind product presents obvious insufficiencies and is unable to perfectly mimic the wind that was truly observed on July 24, 25 and 26, 2007, which partly explains the differences noticed between both Lagrangian residual current fields. The other reasons for these differences are related to ocean modelling inadequacies as a non optimal calibration of the vertical turbulent closure scheme already pointed out in Muller et al. (2007) or to the fact that surface waves are not taken into account. However, these findings support the idea of a Lagrangian residual circulation mainly wind-generated at that time of year 2007. Indeed, offshore, tidal currents are known to be weaker than inshore, and the area under study is rather far from frontal areas, so the wind is the main driving mechanism liable to explain drift processes in the surface layer.

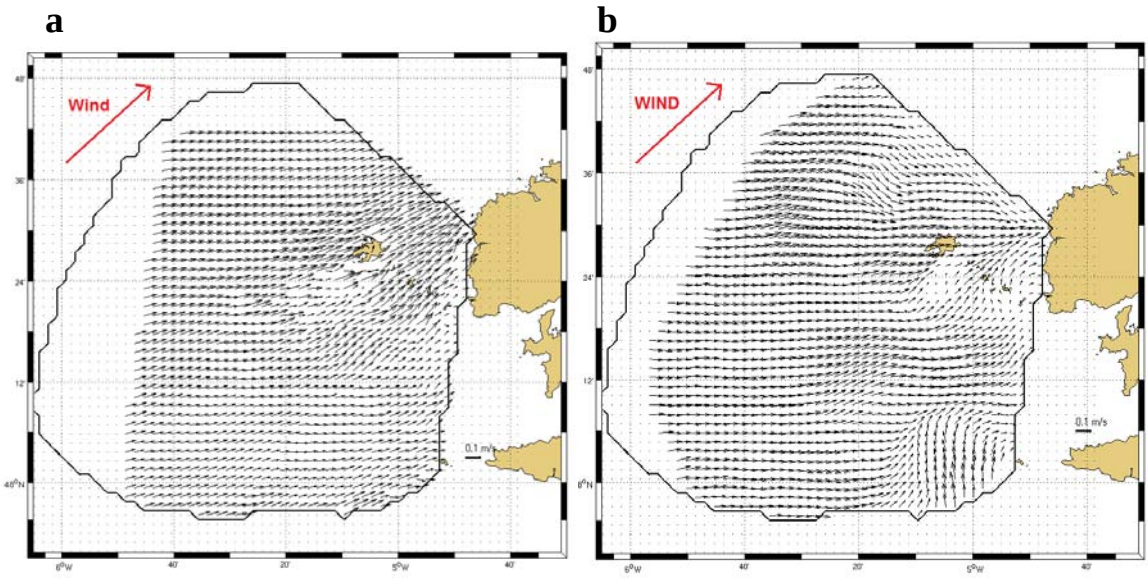

Fig. 18: Lagrangian residual current from (a) MARS results and (b) HF radar data over four tidal cycles from July 24, 2007, 00:00 UTC, with the direction of the mean wind computed with WRF over the same period.

3.3.3 Density-driven residual currents

The contribution of density-driven currents to the Lagrangian residual circulation is more difficult to detect because it is easily masked by strong wind gusts and by the strong residual signal induced by the tidal circulation. This consideration drove us to investigate first and foremost situations that show the presence of the thermal front under calm wind conditions and at neap tide. This was the case on August 8, 2007 and throughout the next four tidal cycles: anticyclonic meteorological conditions were prevailing with weak winds during neap tide conditions. The superimposition of the Lagrangian residual circulation computed from HF radar data over the four tidal cycles on the thermal front diagnosed with an appropriate threshold on the horizontal temperature gradient $\left|\overrightarrow{\nabla_H T}\right| = \sqrt{\frac{\partial T}{\partial x}^2 + \frac{\partial T}{\partial y}^2}$ (where H means horizontal and T stands for temperature) shows, indeed, the density-driven residual circulation (Figure 19). Salinity variations are very weak nearby and across the frontal area during summer (Birrien, 1987). Therefore, one can infer density-currents directly from temperature fronts. The northward and the southward along-front movements (see part 1.3.3) appear, respectively, in the homogeneous and stratified areas, nearby 5°20'. It is worth noting that a thorough examination of Figures 16 and 17 reveals such opposite water displacements in the frontal regions. Baroclinic instabilities also develop in the frontal area and generate meanders, and even residual eddies such as the one noticeable at 5°20'W, 48°12'N (Figure 19). The attractive nature of the front expresses itself in the direction of the Lagrangian residual current on each side of the front. A local calculation of the horizontal divergence of the residual circulation would allow one to evidence this feature.

We also performed some Lagrangian integrations from MARS model outputs and checked the propensity of some numerical drifters to follow the thermal front as already inferred from observations (see part 1.3.3). Figure 20 illustrates the superimposition of some relevant positions of a numerical drifter on the MARS-computed sea surface temperature

(SST) at the same date; it confirms the ability of MARS to reproduce the southward residual surface circulation in the stratified area nearby the front.

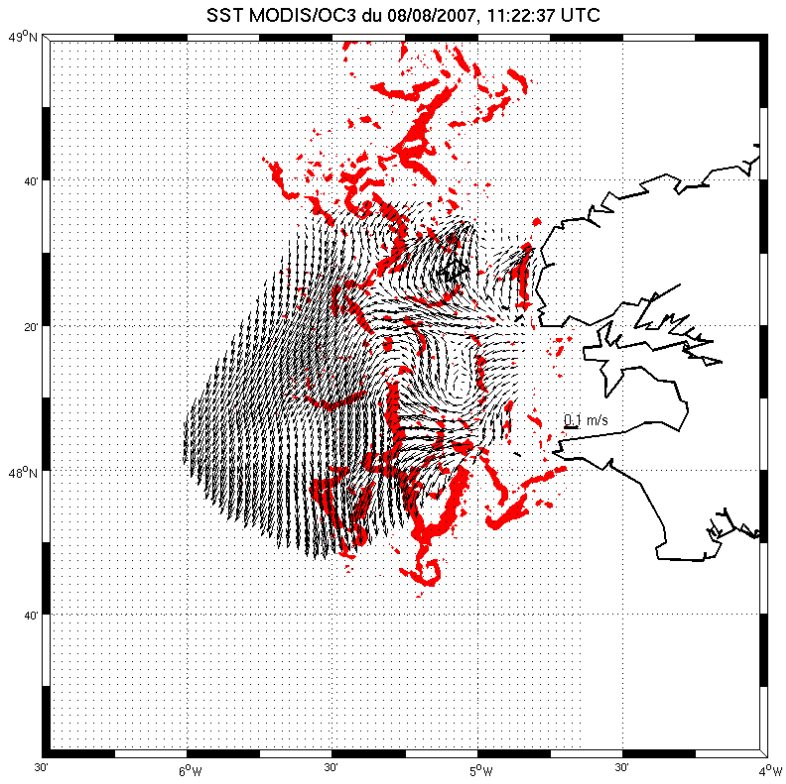

Fig.19: Tidal front location (contours in red of the $3.10^{-4}°C/m$ value of the horizontal temperature gradient) on August 8, 2007, 11:22 UTC together with the Lagrangian residual current (arrows) deduced from HF radar data over four tidal cycles from August 8, 2007, 00:00 UTC.

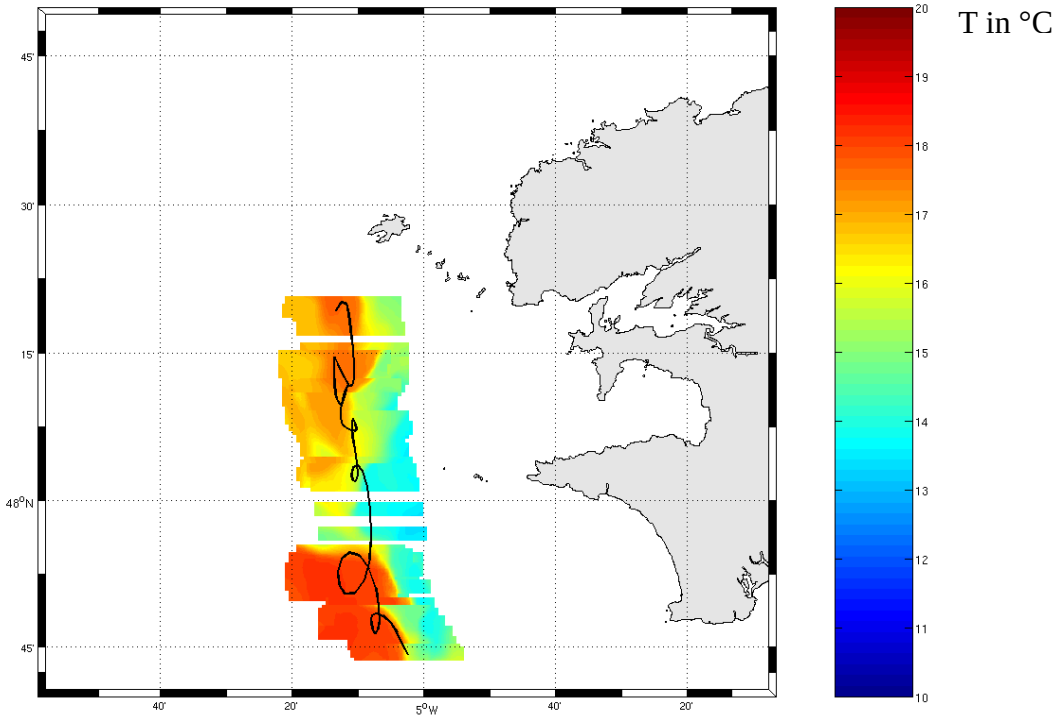

Fig. 20: Full 2-day trajectory of a numerical drifter released in the MARS surface velocity field, and concomitant MARS SST field for a few selected dates.

Conclusion

This paper provided a new description of the Lagrangian residual circulation in the Iroise Sea and underlined the different physical mechanisms that govern it. From the available large spectrum of data describing the hydrodynamics of the area (surface currents issued from HF radar measurements, high resolution modelling of the air/sea system, trajectories of several drifters drogued at different depths), our aim was to devise a protocol allowing one to estimate the Lagrangian residual circulation over relevant periods. Our approach consisted in computing the Lagrangian residual current from two different points of view. The former is a theoretical calculation based on the Longuet-Higgins (1969) approximation, whose main objective is to provide a rough estimate of the Lagrangian residual circulation from instantaneous circulation. The latter relies on a diagnostic Lagrangian tool (Blanke and Raynaud, 1997) that computes full trajectories of fictive particles advected in a given velocity field. This analysis was applied to the outputs of ocean models and to gridded currents derived from HF radar measurements. Both sources of data are indeed complementary to study the Lagrangian residual circulation according to the impact of the physical processes at play. The calculated Lagrangian residual currents were compared to real Lagrangian drifters released in the Iroise Sea.

The method reported here should contribute to a better understanding of transport problems in many other areas where Lagrangian residual circulation is a source of concern, like, for example, in the vicinity of the Channel islands where the dispersal of radionuclides released from the AREVA La Hague spent fuel reprocessing plant is a key issue (Bailly du Bois and Dumas, 2005), or in the Bohai Sea where the Lagrangian residual currents cause deposition of sediments from the Huanghe river along the southern bank of the Bohai Bay (Hao et al., 2004).

Our analysis revealed, however, that the direct comparison of drifter tracks and numerical trajectory calculations (based on modelled or radar-derived sea surface velocities) is difficult and does not provide much insight about the overall quality of the predicted trajectories. This paper dealt only with qualitative comparisons, which revealed some consistency between the Lagrangian residual currents estimated from the different sources of data; on the other hand, the difficulty to find identical structures at the same place and time prevented us from making attempt to quantify differences or similarities.

In future investigations, focus will be on enhancement of the modelling of the instantaneous hydrodynamics in the region of interest so as to provide enhanced Lagrangian diagnostics. In particular, it is critical to investigate to which extent the Lagrangian residual circulation is affected by the spatio-temporal variability of the physical processes. The use of available HF radar data is expected to help in the determination of differences between winter and summer Lagrangian residual structures.

It also sounds to us worth focusing, in the future, on the incorporation of the concept of Lagrangian Coherent Structures (LCSs) into our Lagrangian diagnostics. Lagrangian Coherent Structures are attractive and repulsive lines in the ocean and give a geometrical representation of the mean circulation (Shadden et al., 2005, Lekien and Coulliette, 2007). On condition to be used with appropriate parameters, they provide us with a skeleton of the Lagrangian residual circulation of the Iroise Sea. A set of LCSs corresponds to each velocity field whatever its origin, i.e. issued from HF radar data or output of an ocean model. The differences between LCSs permit a quantification of the differences between the two velocity fields from the Lagrangian point of view.

Acknowledgements: We acknowledge the ACTIMAR company for its financial support and for the high-frequency radar data put at our disposal within the context of the SURLITOP project initiated within the framework of the RITMER network. We are grateful to SHOM (French naval hydrographic and oceanographic service) who provided the bathymetry data. We thank Marie-Paule Friocourt for assistance in the manuscript corrections. Numerical calculations were performed with the computational resources available at the Centre de Brest of IFREMER.

References

Arakawa A, Lamb VR (1977) Computational design of the basic dynamical processes of the UCLA general circulation model. Meth Comput Phys 17:173-265

Ardhuin F, Martin-Lauzer F-R, Chapron B, Craneguy P, Girard-Ardhuin F, Elfouhaily T (2004) Wave-induced drift at the ocean surface. C.R. Geoscience 336:1121-1130

Bailly du Bois P., Dumas F. (2005), Fast hydrodynamic model for medium- and long-term dispersion in seawater in the English Channel and southern North Sea, qualitative and quantitative validation by radionuclide tracers. Ocean Modelling Vol 9/2 pp 169-210.

Birrien J.L. (1987) Cycles de variations des éléments nutritifs et du phytoplancton en baie de Douarnenez et dans les secteurs adjacents : Importance du front côtier de l'Iroise. Thèse de doctorat, Université de Bretagne Occidentale, faculté des sciences et techniques, Brest

Blanke B, Raynaud S. (1997) Kinematics of the Pacific Equatorial Undercurrent: a Eulerian and Lagrangian approach from GCM results. J. Phys. Oceanogr., **27**, 1038-1053

Cheng R.T., Casulli V. (1982) On lagrangian residual currents with applications in South San Francisco Bay, California, Water Resour. Res., 18(6), 1652-1662

Cochin V. (2006) Evaluation of ground wave HF/VHF radars for operational oceanography. Ph.D. thesis, National School of Telecommunications of Brittany, France

Copeland A.C., Ravichandran G., Trivedi M.M. (1995) Localized Radon transform-based detection of ship wakes in SAR images, IEEE Trans.Geosci. Remote Sensing, .Vol. 33, no. 1

Debreu L., Vouland C., Blayo E. (2005) AGRIF :Adaptative Grid Refinement in Fortran, Computers and Geosciences

Delhez E. (1996) On the residual advection of the passive constituents. J. Mar. Syst. 8, pp. 147-169

Demerliac A (1973) Calcul du niveau moyen journalier de la mer. Rapport du service hydrographique de la marine

Faugère Y., Le Borgne P., Roquet H. (2001) Réalisation d'une climatologie mondiale de la température de surface de la mer à échelle fine. Météo France, Direction de la production, Centre de Météorologie Spatiale. La Météorologie 35.

Feldman G.C, McClain C.R, Ocean Color Web, MODIS Reprocessing, NASA Goddard Space Flight Center. Eds. Kuring, N., Bailey, S.W. http://oceancolor.gsfc.nasa.gov

Feng S. (1986) A three-dimensional weakly nonlinear dynamics on tide-induced Lagrangian residual current and mass-transport, Chinese J. of Oceanology and Limnology, vol 4, 2, 139-158

Gurgel K.-W, Antonischki G., Essen H.-H, Schlick T. (2000) Wellen Radar (WERA): a new ground-wave HF radar for ocean remote sensing. Coastal Engineering.

Hao W., Hainbucher D., Pohlmann T., Feng S., Suendermann J. (2004) Tidal-induced Lagrangian and Eulerian mean circulation in the Bohai Sea. J.mar.syst., vol. 44, n°3-4, pp. 141-151.

Jenkins A.D. (1987) Wind and wave induced currents in a rotating sea with depth-varying eddy viscosity, J. Phys. Oceanogr. 17: 938-951

Kaplan D.M, Lekien F. (2007) Spatial interpolation and filtering of surface current data based on open-boundary modal analysis. Journal of Geophysical Research, 112, Art. no. C12007.

Lazure P, Dumas F (2007) An external-internal mode coupling for a 3D hydrodynamical model for applications at regional scale (MARS). Adv Water Resour

Lekien F., Coulliette C. (2007) Chaotic stirring in quasi-turbulent flows, Philosophical Transactions of the Royal Society, 365(1861): 3061-3084.

Lekien F., Coulliette C., Bank R., Marsden J. (2004) Open-boundary modal analysis: Interpolation, extrapolation, and filtering. Journal of Geophysical Research, 109, Art. no. C12004.

Longuet-Higgins M. S. (1969) On the transport of mass by time-varying ocean currents. Deep-Sea Res., **16**, 431–447

Luyten P., De Mulder T. (1992) A module representating surface fluxes of momentum and heat, MUMM's technical report#9, 30pp.

Lyard F., Lefèvre F., Letellier T., Francis O. (2006) Modelling the global ocean tides : modern insights from FES 2004. Ocean Dynamics. Volume 56, Numbers 5-6, 394-415

Mariette V, Le Corre P (1982) Le front thermique d'Ouessant en août et septembre 1982, campagne Satir Dynatlant. Campagne océanographique française no. 1-1985. IFREMER, France

Mariette V (1983) Effet des échanges atmosphériques sur la structure thermique marine. Application à des zones du large et à une zone côtière. Thèse de doctorat ès Sciences Physiques, Université de Bretagne Occidentale, Brest

Mariette V., Le Saos J.P., Rougier G. (1983) Résultats des mesures d'océanographie physique réalisées lors de la campagne Satir-Dynatlant. Rapport scientifique. Laboratoire de Physique des Océans. Université de Bretagne Occidentale, Brest.

Muller H, Dumas F, Blanke B, Mariette V (2007) High-resolution atmospheric forcing for regional oceanic model: the Iroise Sea. Ocean Dynamics

Orbi A, Salomon J.C. (1988) Dynamique de marée dans le golfe normand-breton, Oceanologica Acta vol 11, N°1

Penven P., Debreu L., Marchesiello P., McWilliams J.C. (2004) Applications of the ROMS embedding procedure for the Central California Upwelling System, Ocean Modelling, 12:157-187

Salomon J.C, Breton M. (1993a) An atlas of long term currents in the Channel. Oceanol. Acta, 16(5-6): 439-448

Salomon J.C, Guéguéniat P, Orbi A, Baron Y (1988) A Lagrangian model for long-term tidally-induced transport and mixing. Verification by artificial radionuclide concentrations. Radionuclides: a tool for oceanography. Elsevier Applied Science, 384-394

Shadden S.C., Lekien, F., Marsden, J.E. (2005) Definition and properties of Lagrangian coherent structures from finite-time Lyapunov exponents in two-dimensional aperiodic flows. Physica D, 212 (3-4): 271—304.

Zimmerman J. T. F. (1979) On the Euler-Lagrangian transformation and the Stokes drift in the presence of oscillatory and residual currents, Deep Sea Res., 26 A, 505-520

Figure legends

Fig. 1: Map of the Iroise Sea and Finistère with the location of the transect (in black) realised during the Fromvar campaign in September 2007 (see part 1.3.3)

Fig. 2: Streamlines obtained from tidal residual currents following Salomon (1988)

Fig. 3: Full (blue) and filtered (black) trajectories of drifters (a) 72970 and (b) 72980, both drogued at a 15-m depth

Fig. 4: Filtered trajectories (green) of surface drifter 72994 and WRF wind vectors (blue)

Fig. 5: Time evolution of the drift velocity of surface drifter 72994 (red) and 2% of the wind speed (green) for (a) u- and (b) v-components

Fig. 6: Vertical temperature structure (in °C) across the Iroise Sea at 48.15°N (see Figure 1) measured during the Fromvar campaign (September 2007) and orientation of the density-driven currents from the thermal wind equations.

Fig. 7: SST (colour palette) and full (red) and filtered (black) trajectory of drifter 24568

Fig.8: Surface currents estimated by raw pointwise recombination of HF radar data (red) and surface currents reconstructed with OMA (black) on September 5, 2005, 02h48; Brezellec and Garchine are the radars' locations.

Fig. 9: Collocated HF Radar (red + symbol) and real subsurface drifter (blue + symbol) velocities showing the tidal ellipse over 5 days. Dashed segments connecting the radar and drifter velocities indicate the difference (bias) between the two velocity estimates.

Fig. 10: Relative ratio of the mean Lagrangian and Eulerian velocity magnitudes $\frac{U_L - \overline{U_{eulerian}}^T}{\overline{U_{eulerian}}^T}$, $U_{eulerian}$ is the norm of the Eulerian residual current and U_L is the norm of the Lagrangian residual current (note: the colour palette is saturated)

Fig. 11: Angle in degrees between the Lagrangian and Eulerian mean velocities $\left(\theta = sign(\overrightarrow{u_{lagrangian}} \times \overrightarrow{u_{eulerian}}) \times arc\cos(\frac{\overrightarrow{u_{eulerian}} . \overrightarrow{u_{lagrangian}}}{\left\| \overrightarrow{u_{eulerian}} \right\| . \left\| \overrightarrow{u_{lagrangian}} \right\|}) \right)$

Fig. 12: Difference between the Lagrangian and Eulerian mean zonal velocities ($u_L - \overline{u_{eulerian}}^T$, in m/s) computed with (a) ARIANE and (b) Longuet-Higgins theoretical approach; area with strong non linearities is hidden in the b panel.

Fig. 13: Same as Figure 12 except for the mean meridional velocities

Fig. 14: Zonal component of the Lagrangian residual current calculated from (a) raw radar data, (b) OMA-post-processed radar data, (c) MARS results, computed over a M2 tidal cycle from September 12, 2005, 21:11:00 UTC; the black contour represents the HF radar coverage.

Fig. 15: Same as Figure 14 except for the meridional component of the residual current.

Fig. 16: MARS Lagrangian residual current over one tidal cycle from September 18, 2005, 00:00 UTC.

Fig. 17: HF-radar-derived Lagrangian residual current over one tidal cycle from September 18, 2005, 00:00 UTC.

Fig. 18: Lagrangian residual current from (a) MARS results and (b) HF radar data over four tidal cycles from July 24, 2007, 00:00 UTC, with the direction of the mean wind computed with WRF over the same period.

Fig. 19: Tidal front location (contours in red of the $3.10^{-4}°C/m$ value of the horizontal temperature gradient) on August 8, 2007, 11:22 UTC together with the Lagrangian residual current (arrows) deduced from HF radar data over four tidal cycles from August 8, 2007, 00:00 UTC.

Fig. 20: Full trajectory of a numerical drifter released in the MARS surface velocity field, and concomitant MARS SST field for a few selected dates.